Title

Targeted Overexpression of Mitochondrial Catalase Prevents Radiation-Induced Cognitive Dysfunction

Journal

Antioxidants & Redox Signaling, 22(1)

ISSN

1523-0864

Authors

Parihar, Vipan K

Allen, Barrett D

Tran, Katherine K

et al.

Publication Date

2015

DOI

10.1089/ars.2014.5929

Peer reviewed

ANTIOXIDANTS & REDOX SIGNALING
Volume 22, Number 1, 2015

DOI: 10.1089/ars.2014.5929

Discoveries

ORIGINAL RESEARCH COMMUNICATION

Targeted Overexpression of Mitochondrial Catalase Prevents Radiation-Induced Cognitive Dysfunction

Vipan K. Parihar,[1] Barrett D. Allen,[1] Katherine K. Tran,[1] Nicole N. Chmielewski,[1] Brianna M. Craver,[1] Vahan Martirosian,[1] Josh M. Morganti,[2] Susanna Rosi,[2,3] Roman Vlkolinsky,[4] Munjal M. Acharya,[1] Gregory A. Nelson,[4] Antiño R. Allen,[5] and Charles L. Limoli [1]

Abstract

Aims: Radiation-induced disruption of mitochondrial function can elevate oxidative stress and contribute to the metabolic perturbations believed to compromise the functionality of the central nervous system. To clarify the role of mitochondrial oxidative stress in mediating the adverse effects of radiation in the brain, we analyzed transgenic (mitochondrial catalase [MCAT]) mice that overexpress human catalase localized to the mitochondria. ***Results:*** Compared with wild-type (WT) controls, overexpression of the MCAT transgene significantly decreased cognitive dysfunction after proton irradiation. Significant improvements in behavioral performance found on novel object recognition and object recognition in place tasks were associated with a preservation of neuronal morphology. While the architecture of hippocampal CA1 neurons was significantly compromised in irradiated WT mice, the same neurons in MCAT mice did not exhibit extensive and significant radiation-induced reductions in dendritic complexity. Irradiated neurons from MCAT mice maintained dendritic branching and length compared with WT mice. Protected neuronal morphology in irradiated MCAT mice was also associated with a stabilization of radiation-induced variations in long-term potentiation. Stabilized synaptic activity in MCAT mice coincided with an altered composition of the synaptic AMPA receptor subunits GluR1/2. ***Innovation:*** Our findings provide the first evidence that neurocognitive sequelae associated with radiation exposure can be reduced by overexpression of MCAT, operating through a mechanism involving the preservation of neuronal morphology. ***Conclusion:*** Our article documents the neuroprotective properties of reducing mitochondrial reactive oxygen species through the targeted overexpression of catalase and how this ameliorates the adverse effects of proton irradiation in the brain. *Antioxid. Redox Signal.* 22, 78–91.

Introduction

THE ADVERSE EFFECTS of cranial irradiation on central nervous system (CNS) functionality have long been recognized. Patients subjected to radiotherapy for the control of primary and metastatic brain tumors routinely exhibit progressive and debilitating cognitive impairments that are known to adversely impact quality of life (10, 15, 43). The affected cognitive domains are diverse and include disrupted learning, memory, processing speed, attention, and executive function (43, 44). While radiotherapy is designed to deliver curative doses in excess of 45 Gy, neurocognitive sequleae are elicited at much lower doses (≤ 10 Gy), doses typically far below the threshold for detecting overt normal tissue injury (*i.e.*, radionecrosis) (20, 64). Outside of the clinical setting, irradiation of the CNS can occur occupationally, including those involved with medical diagnostics, the nuclear power industry, or those engaged in space travel (8, 12, 16, 52). In these circumstances, total doses are much lower (≤ 2 Gy), and for astronauts, absorbed doses are derived from

[1]Department of Radiation Oncology, University of California, Irvine, Irvine, California.
[2]Departments of Physical Therapy Rehabilitation Science and Neurological Surgery, University of California, San Francisco, San Francisco, California.
[3]Brain and Spinal Injury Center, University of California, San Francisco, San Francisco, California.
[4]Departments of Radiation Medicine and Basic Sciences, Loma Linda University, Loma Linda, California.
[5]Division of Radiation Health, University of Arkansas Medical School, Little Rock, Arkansas.

Innovation

Radiation-induced cognitive dysfunction is a serious complication associated with cranial radiation exposure. While this problem has long been recognized, no satisfactory interventions for this debilitating condition exist, which is further complicated by an incomplete understanding of the underlying mechanisms. Here, we provide evidence that a genetic manipulation designed to reduce mitochondrial oxidative stress significantly improves cognition after proton irradiation. Importantly, improved cognitive performance was associated with a preservation of neuronal morphology and a stabilization of long-term potentiation in the irradiated hippocampus. These data stress the importance of redox homeostasis in the irradiated brain, involved in protecting and maintaining neuronal structure and central nervous system functionality.

the traversal of energetic charged particles (protons, heavy ions) comprising the space radiation environment (12, 16). Charged particles possess different energy deposition properties from photon radiation, and several recent studies investigating the effects of charged particles on the CNS have found significant cognitive deficits after very low-dose exposures (5–30 cGy) (9, 39, 65). Despite inherent differences between radiation types and total absorbed dose, the capability of clinical and occupational radiation exposure to significantly compromise cognition are clearly problematic, and suggest that free radical mechanisms initiated by irradiation serve to disrupt the fundamental structure of the CNS to impair function.

The precise mechanisms underlying radiation-induced cognitive dysfunction remain largely unresolved, suggesting a need to further understand radiation effects in the CNS. Exposure to ionizing radiation initiates a cascade of free radical reactions that are largely complete within milliseconds (67, 68). This relatively instantaneous insult, however, can lead to acute cellular changes that last from minutes to days, or more persistent changes which can last for months or even years when considering the adverse cognitive consequences associated with irradiation of the CNS. While the burst of reactive species generated during interactions between the incident particles and tissue are short lived, significant work has shown that reactive oxygen species (ROS) and reactive nitrogen species can be generated over extended postirradiation times (weeks to months), through a variety of metabolic perturbations that can be linked to mitochondrial dysfunction (32, 37, 65). The onset and persistence of radiation-induced oxidative stress has been shown to impact a wide range of biologic endpoints, and has a particularly pronounced effect in the CNS, where changes in redox state are accompanied by alterations in stem cell proliferation and differentiation that impact neurogenesis (21, 56–58). To expand on these observations and directly assess the importance of mitochondrial oxidative stress in the CNS, we utilized a transgenic mouse model (mitochondrial catalase [MCAT]) engineered to overexpress human catalase targeted to the mitochondria. Mice overexpressing the MCAT transgene have been shown to exhibit lifespan extension (59) and reduced pathology associated with aging (13). More recently, MCAT mice were shown to exhibit improved neurogenesis before and after proton irradiation, suggesting a potential neuroprotective role for reducing mitochondrial oxidative stress (35). To follow up on these observations, and more completely elucidate the functional importance of MCAT overexpression in the proton irradiated brain, we have undertaken a series of rigorous cognitive testing studies coupled with neuronal morphometry, *in vitro* electrophysiological testing of synaptic plasticity (long-term potentiation [LTP]), and biochemical assessments of AMPA receptors.

Hydrogen peroxide has been shown to be a potent neurotoxin that mediates oxidative damage and injury to multiple neural cell types caused by disease, aging, neurodegeneration, stress, and irradiation (18, 34, 40, 45, 47). Hydrogen peroxide can be generated from several intracellular sites, including the mitochondria, where the mitochondrial isoform of superoxide dismutase (SOD)2 converts superoxide derived from leaky electron transport to hydrogen peroxide (25). Therefore, the capability to attenuate this powerful prooxidant at a primary intracellular source provided the means for directly testing the functional importance of mitochondrial oxidative stress on multiple CNS endpoints after irradiation. Furthermore, our group has recently found that proton or gamma-ray irradiation elicits significant changes in neuronal anatomy and synaptic integrity (11, 50, 51). Persistent reductions in dendritic complexity and spine density were coincident with alterations in spine morphology and pre and postsynaptic protein levels, changes that were temporally coincident with impaired cognition. These findings suggested the possibility that some of the neuroprotective properties associated with overexpression of the MCAT transgene might be linked to the preservation of neuronal morphology and/or the maintenance of synaptic integrity and function. Here, we report our new findings showing the beneficial cognitive effects of the MCAT transgene after proton irradiation, along with a comprehensive series of morphometric, biochemical, and electrophysiological analyses designed to elucidate the mechanistic basis of neuroprotection in MCAT mice.

Results

Antioxidant status of MCAT mice

Past studies have characterized the antioxidant properties of MCAT mice (13, 59). Our past work has confirmed that catalase activity was significantly elevated in the cortex, amygdala, hippocampus, and cerebellum of MCAT mice (49) and showed that neural tissue from MCAT mice exhibited significantly lower (twofold) levels of lipid peroxidation compared with wild-type (WT) mice when exposed to hydrogen peroxide (35). To confirm the activity of catalase (m*k* units/mg) in the current set of cohorts, brains from WT and MCAT mice were prepared for catalase activity assays (70). These data re-confirmed that MCAT mice had 10-fold higher levels of catalase activity (11.4 ± 3.23) compared with WT mice (1.03 ± 0.206). These values did not change significantly over the range of proton dose used in this study (data not shown).

Behavioral performance

Novel object recognition. Mice were habituated and then tested on the novel object recognition (NOR) arena at 1 month postirradiation. Successful performance on this task is

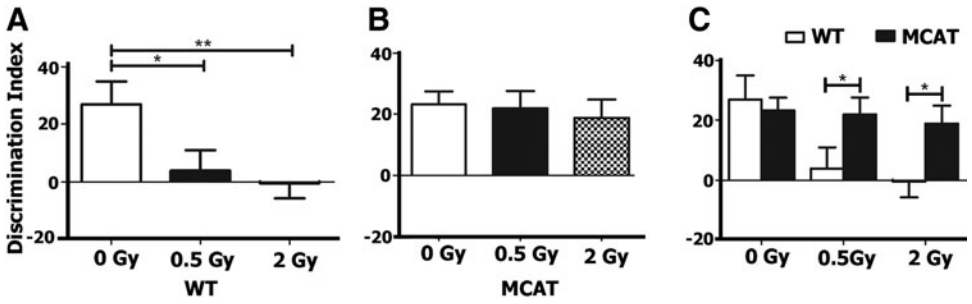

FIG. 1. NOR in WT and MCAT mice. Episodic memory retention measured using the NOR task at 1 month post-proton irradiation. **(A)** WT mice show behavioral deficits when exposed to radiation at 0.5 Gy (*$p < 0.05$, unpaired *t*-test) and 2.0 Gy (**$p < 0.01$, unpaired *t*-test) when compared with controls. **(B)** Irradiated MCAT mice show no significant ($p > 0.05$) differences when compared with MCAT controls. **(C)** Mice overexpressing MCAT show significant preference for the novel object when compared with 0.5 Gy WT mice (*$p < 0.05$, unpaired *t*-test) and at 2.0 Gy (*$p < 0.05$, unpaired *t*-test). All data were derived from 16 animals and plotted as the mean ± SEM. MCAT, mitochondrial catalase; NOR, novel object recognition; WT, wild type.

dependent on intact prefrontal cortex and hippocampal function (2, 6). Impairment in these brain regions manifests as an inability to discriminate a novel from a familiar object (2, 6). To quantify preference or indifference for exploring novelty, a discrimination index was calculated. A positive score indicates a preference, or more time exploring the novel object, while a negative score indicates indifference, or more time exploring the familiar object. After exposure to a novel object for 5 min, WT control mice showed a preference for the novel object (Fig. 1). However, when WT control mice were irradiated at 0.5 and 2.0 Gy, this preference was significantly diminished [$F_{(1,42)} = 4.686$, $p = 0.014$, ANOVA] (Fig. 1A). When mice overexpressing MCAT were exposed to the same test, no significant differences were found between control and irradiated groups [$F_{(1,40)} = 0.17$, $p = 0.84$, ANOVA] (Fig. 1B). A comparison of WT to MCAT mice found no significant differences between control groups ($p = 0.70$, unpaired *t*-test), while irradiated WT mice exhibited significant impairments in NOR after doses of 0.5 Gy ($p = 0.05$, unpaired *t*-test) and 2.0 Gy ($p = 0.02$, unpaired *t*-test) (Fig. 1C).

Object in place. After NOR testing, mice were habituated and tested in the object in place (OiP) arena. This test is also dependent on intact function of the hippocampus in addition to the prefrontal and perirhinal cortices (2, 6). Mice having intact cortical function will show a preference toward the objects that have been switched to a novel location. As expected, WT control mice exhibited a strong preference for the objects placed at novel locations (Fig. 2A). Both WT irradiated groups showed almost no preference for any of the objects and exhibited significant decrements compared with sham irradiated controls [$F_{(1,43)} = 5.393$, $p = 0.008$, ANOVA] (Fig. 2A). All irradiated groups of MCAT mice showed a strong preference for the switched objects with no significant differences between irradiated and control groups [$F_{(1,44)} = 0.96$, $p = 0.39$, ANOVA] (Fig. 2B). Both WT and MCAT control groups showed an equivalent preference for the switched object ($p = 0.57$, unpaired *t*-test), while irradiated WT mice scored significantly lower than MCAT mice at both 0.5 Gy ($p = 0.02$, unpaired *t*-test) and 2.0 Gy ($p = 0.03$, unpaired *t*-test) doses (Fig. 2C).

Morphometric analyses of hippocampal neurons

For morphological quantification of hippocampal neurons, we measured length and branching of the granule cells in the dentate gyrus (DG) and pyramidal neurons in the CA1 region from six MCAT and six WT mice. Representative images of hippocampal sections show the types of Golgi-Cox impregnated neurons used for morphometric analyses (Supplementary Fig. S1A–C; Supplementary Data are available online at

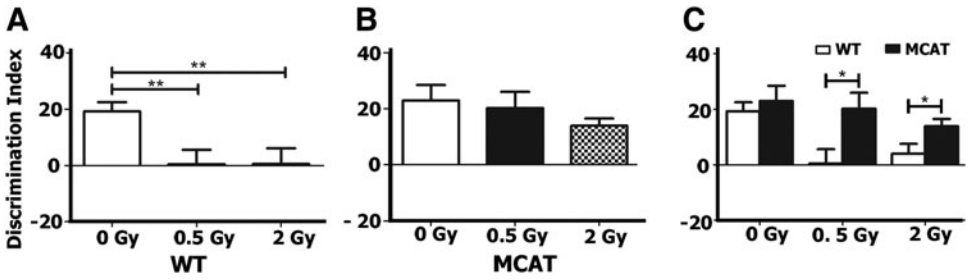

FIG. 2. OiP testing in WT and MCAT mice. Spatial memory retention measured using the OiP test at 1 month post-proton irradiation. **(A)** WT mice show behavioral deficits when exposed to radiation at 0.5 Gy (**$p < 0.005$, unpaired *t*-test) and 2.0 Gy (**$p < 0.005$, unpaired *t*-test) when compared with WT controls. **(B)** MCAT mice that were irradiated at 0.5 Gy ($p > 0.05$) and 2.0 Gy ($p > 0.05$) show no significant differences compared with MCAT controls. **(C)** MCAT mice show a significant preference for novel placed objects when compared with WT mice irradiated with 0.5 Gy (*$p < 0.05$, unpaired *t*-test) and 2.0 Gy (*$p < 0.05$, unpaired *t*-test). All data were derived from 16 animals and plotted as the mean ± SEM. OiP, object in place.

www.liebertpub.com/ars) and dendritic segments used for the assessment of spine morphology and number (Supplementary Fig. S1D–F). In the DG, unpaired *t*-tests revealed that doses of 0.5 or 2 Gy of protons did not significantly affect total dendritic length (data not shown), total branch points, or dendritic complexity when WT mice were compared with MCAT (Supplementary Fig. S2). To characterize the dendritic branching characteristics of individual neurons, we performed Sholl analysis (60). Two-way repeated analysis of variance (ANOVA) revealed a significant genotype × radius interaction in the DG with 0.5 Gy [$F_{(25,100)} = 1.92$, $p < 0.05$, ANOVA] and 2 Gy [$F_{(25,175)} = 3.00$, $p < 0.0001$, ANOVA], indicating that expression of the MCAT transgene is associated with a different distribution of dendritic branching over the entire tree (Supplementary Fig. S2). *Post hoc* tests showed that MCAT mice had a significant improvement in dendritic branching at regions proximal to the soma (30–60 μm) after a 0.5 Gy dose of protons compared with WT mice (Supplementary Fig. S2). At the higher 2 Gy dose of protons, MCAT mice exhibited significantly increased dendritic branching at regions more distal from the soma (130–170 μm, Supplementary Fig. S2).

A similar analysis was performed on the basal and apical regions of the CA1 pyramidal neurons. No significant differences were noted in total branch points, dendritic length, or dendritic complexity between WT and MCAT mice at 0 or 0.5 Gy along basal (Supplementary Fig. S3) or apical (Supplementary Fig. S4) regions of the dendritic tree. Sholl analysis revealed some increased apical branching that was significant between unirradiated controls and MCAT mice at proximal distances from the soma (50–60 μM, Supplementary Fig. S4). In the basal regions, a 2 Gy exposure of protons significantly reduced the total number of branch points ($p < 0.01$), dendritic length ($p < 0.05$), and dendritic complexity ($p < 0.05$) in WT mice (Fig. 3A). In MCAT mice given this same dose, reductions in the same dendritic parameters were not found (Fig. 3A). Sholl analyses of these neurons showed that MCAT mice had significantly more dendritic intersections distal to the soma (60–100 μm), while WT mice had increased dendritic branching more proximal to the soma (20–30 μm) (Fig. 4A). At the 2 Gy dose of protons, Sholl analysis revealed a significant genotype × radius interaction [$F_{(15,105)} = 4.89$, $p < 0.001$, ANOVA] for the basal dendritic tree (Fig. 4A).

In the apical regions, exposure to 2 Gy of protons again significantly reduced the total dendritic length ($p < 0.05$), the number of branch points ($p < 0.05$), and dendritic complexity ($p < 0.05$) in WT mice (Fig. 3B). As earlier, MCAT animals did not show these same radiation-induced reductions in structural dendritic parameters. Sholl analysis of the apical dendritic tree revealed a significant genotype × radius interaction [$F_{(25,175)} = 2.25$, $p < 0.001$, ANOVA] at the 2 Gy dose of protons (Fig. 4B). *Post hoc* analysis also revealed that 2 Gy of protons significantly reduced dendritic arborization between 30–40 and 70–100 μm from the soma when WT mice were compared with MCAT animals (Fig. 4B). Representative tracings of CA1

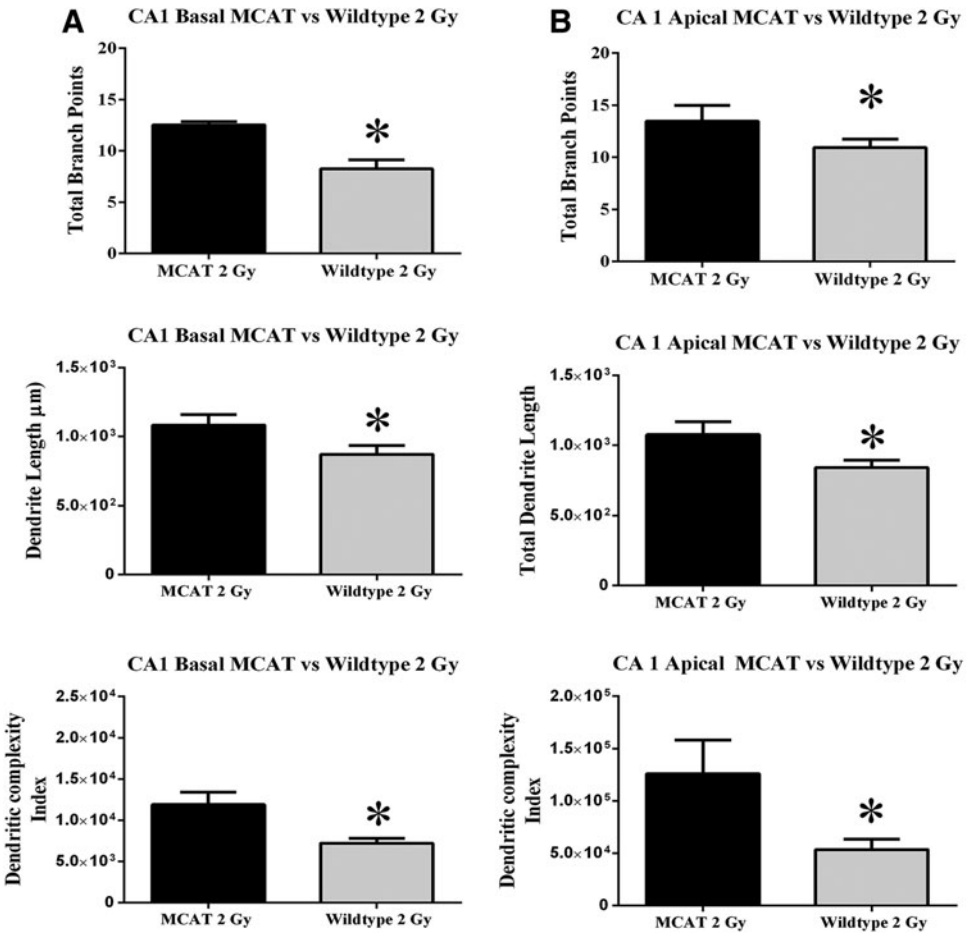

FIG. 3. Dendritic analyses of proton-irradiated CA1 pyramidal neurons in WT and MCAT mice. Morphometric analyses of Golgi-stained neurons at 6 weeks after irradiation enabled the quantification of dendritic branching, length, and complexity. Analysis of basal **(A)** and apical **(B)** dendritic trees of CA1 pyramidal cells revealed that neurons from proton-irradiated (2 Gy) WT mice exhibited significant reductions in the number of branch points, total length, and dendritic complexity when compared with neurons from irradiated MCAT mice. Overexpression of the MCAT transgene was found to preserve dendritic complexity after a 2 Gy proton dose. Error bars represent the mean ± SEM ($n = 6$ animals, three sections per animal, ~50 neurons per cohort). *$p < 0.05$, unpaired two-tailed *t*-test with Welch's correction.

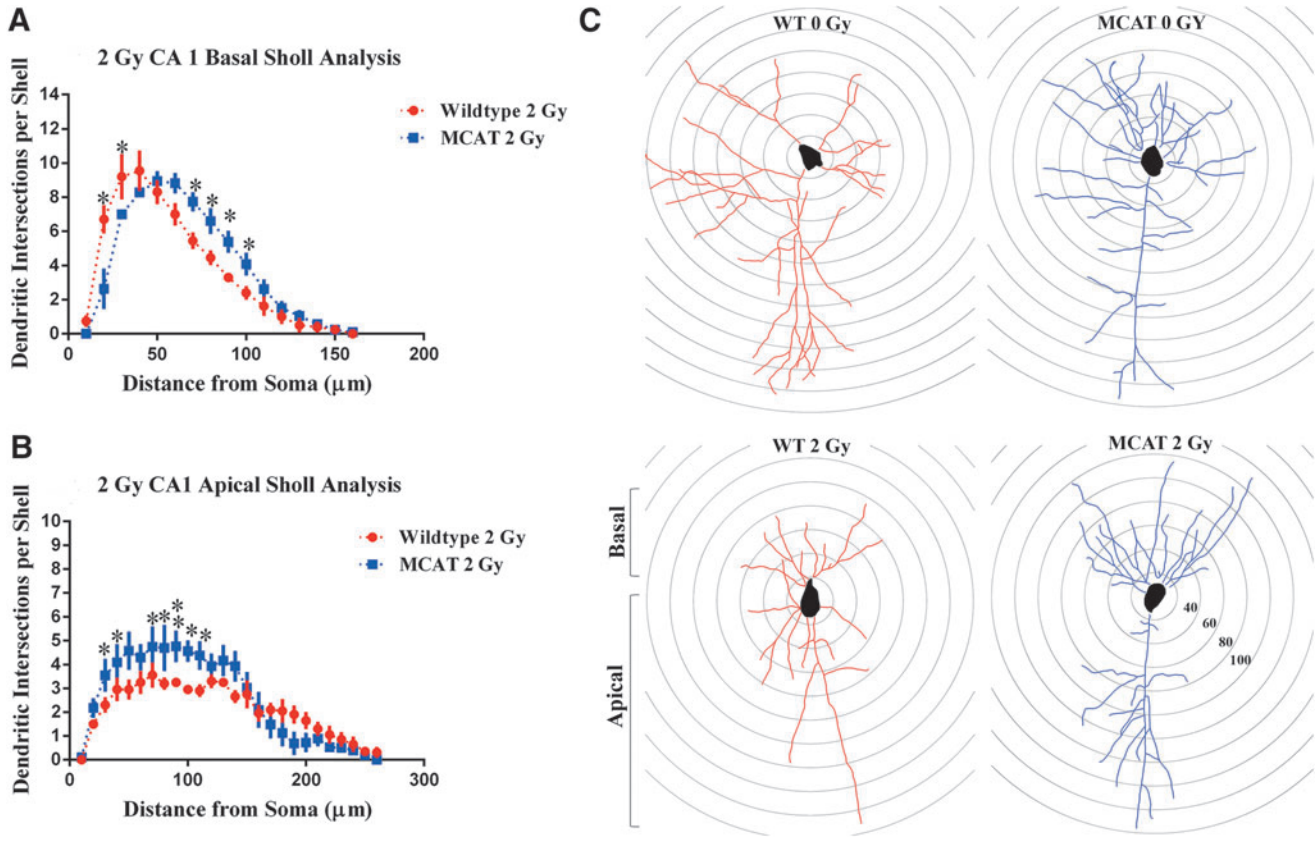

FIG. 4. Sholl analyses of CA1 pyramidal neurons in WT and MCAT mice 6 weeks after proton irradiation. (A) Dendritic intersections measured by Sholl analysis revealed that exposure to 2 Gy of protons significantly reduced the number of dendritic intersections in the basal dendritic tree 70–100 μm from the cell soma when WT mice were compared with MCAT mice. **(B)** Similar analyses performed in the apical dendritic tree showed that irradiation significantly reduced the number of dendritic intersections 30–40 μm and 70–110 μm from the soma when WT mice were compared with MCAT mice. Neurons from MCAT mice routinely exhibited increased dendritic arborization at extended distances from the soma after irradiation with 2 Gy of protons. Error bars represent the mean ± SEM ($n = 6$ animals, three sections per animal, ~50 neurons per cohort). **(C)** Representative tracings of CA1 pyramidal neurons superimposed over concentric rings (20 μM) used for Sholl analyses show typical basal and apical branching patterns. *$p < 0.05$; **$p < 0.01$, mixed factors ANOVA followed by Fisher's LSD *post hoc* analysis. ANOVA, analysis of variance; LSD, least significant difference.

pyramidal neurons show typical basal and apical branching patterns from unirradiated (upper panels) and irradiated (lower panels) WT and MCAT mice (Fig. 4C). Significant reductions in dendritic arborization were only found on those neurons from irradiated WT mice (lower left panel, Fig. 4C).

Dendritic spine analysis

To determine whether reductions in dendritic complexity translated to alterations in dendritic spines after proton irradiation, unbiased stereology was used to quantify spine morphology (Fig. 5A, B) and density (Fig. 5C, D) in WT and MCAT mice, respectively. While irradiation induced some fluctuation in spine type, immature (long, mushroom) and mature (stubby) spines were not significantly affected by either irradiation or genotype. Similarly, the total yield of spines in the DG was not significantly altered by irradiation or genotype.

For pyramidal cells in the CA1 of WT mice, proton irradiation caused a dose-independent rise (~2-fold) in the number of immature spines (long, mushroom), while having a negligible effect on the yield of mature spines (stubby) (Fig. 6A). Spines along neurons in the CA1 from MCAT mice showed little effect of irradiation (Fig. 6B). A compilation of total spine counts in the CA1 revealed dendritic spine density to increase (albeit not significantly) after irradiation in WT mice (Fig. 6C). MCAT mice showed smaller radiation-induced changes in spine density (Fig. 6D). In sum, changes in spine morphology and yield quantified on neurons located within the DG or CA1 were not found to significantly differ between either genotype or after proton irradiation (Figs. 5 and 6).

Electrophysiological assessment of proton irradiated mice

LTP of the dendritic field excitatory postsynaptic potentials (fEPSPs) was induced by presynaptic stimulation (Schaeffer collaterals) using high-frequency stimulation (HFS) delivered at time "0." WT mice exposed to either 0.5 or 1 Gy of protons exhibited considerable variability in fEPSP peak-to-peak amplitudes (Fig. 7A). In control slices, LTP measured at 30 min after HFS averaged 140% ± 5%. Compared with baseline recordings, an exposure of 0.5 Gy increased LTP to 160% ± 22%, while exposure to 1 Gy was found to reduce the LTP magnitude to 120% ± 22%. Proton irradiation elicted a marked variability in the LTP response of

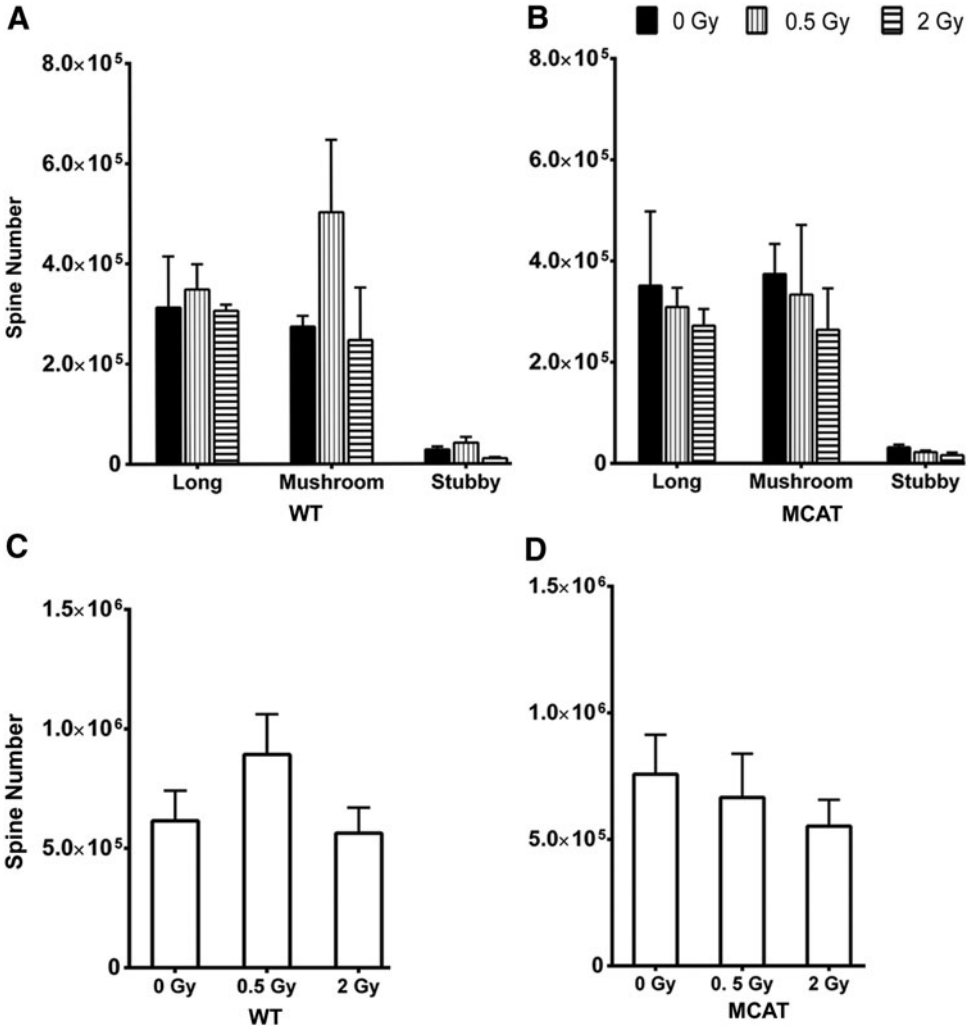

FIG. 5. Spine morphology and density in the DG of WT and MCAT mice. Spine morphology quantified at 6 weeks after proton exposure in WT **(A)** and MCAT **(B)** mice showed little effect of irradiation on either immature (*long*, *mushroom*) or mature (*stubby*) spine types. Overall spine densities did not change significantly after proton irradiation and were not found to differ between WT **(C)** and MCAT mice **(D)**. All data are shown as the mean ± SEM derived from all animals ($n = 3$ animals, three sections per animal). DG, dentate gyrus.

WT mice, an effect that likely precluded data from reaching statistical significance.

Interestingly, the synaptic response of MCAT mice exposed to protons was markedly different. Recordings compared at 30 min after HFS revealed LTP magnitudes in unirradiated and irradiated groups that were nearly identical (Fig. 7B). The LTP magnitudes for all groups plateaued around 140% ± 1% and were statitically indistingusihable throughout the entire course of LTP recording (Fig. 7B). LTP recordings from all MCAT mice matched baseline measurements made in unirradiated WT mice, and indicated a marked stabilizing effect of the MCAT transgene on synaptic responses in CA1 hippocampal neurons.

Synaptosomal analyses

To assess the impact of proton irradiation on synaptic AMPA receptor subunits (AMPARs), synaptosomal fractions containing both presynaptic and postsynaptic membranes were prepared from isolated hippocampi and analyzed for total and phospho-GluR1 and -GluR2 in WT and MCAT animals at 30 days after 0.5 or 2 Gy proton irradiation. Basal levels of either receptor subunit GluR1 or GluR2 did not differ statistically across treatment groups (GluR1 WT sham *vs.* WT 0.5 Gy, $p = 0.4$) (Fig. 8A, B). The basal levels of phosphorylated pGluR1 were significantly increased ($p = 0.03$) in WT animals irradiated with 0.5 Gy compared with sham irradiated animals and compared with 0.5 Gy irradiated MCAT animals (Fig. 8A). The phosphorylated subunit pGluR2 was significantly increased in the MCAT animals irradiated with 0.5 Gy compared with WT irradiated with 0.5 Gy ($p = 0.04$) (Fig. 8B). Both GluR1 and GluR2 are postsynaptic membrane proteins, and levels of syntaxin were assessed to ascertain whether any radiation-induced changes could be found at the presynaptic membrane. No changes in syntaxin were detected across any of the groups (data not shown).

Discussion

Our findings document several neuroprotective properties associated with the targeted overexpression of MCAT. Past and recent work from our laboratory showed a persistent radiation-induced oxidative stress linked to mitochondrial dysfunction which suggested that certain interventions designed to reduce mitochondrial oxidative stress may prove beneficial to a CNS microenvironment known to be prone to oxidative injury (1, 36, 37, 65). The mechanisms by which mitochondrial dysfunction, oxidative stress, and elevated hydrogen peroxide contribute to neuropathology after ischemia, aging, Alzheimer's Disease, and other neurodegenerative conditions have been widely studied (34). Genetic (21, 35, 58, 63), physiologic (38, 47), or pharmacologic

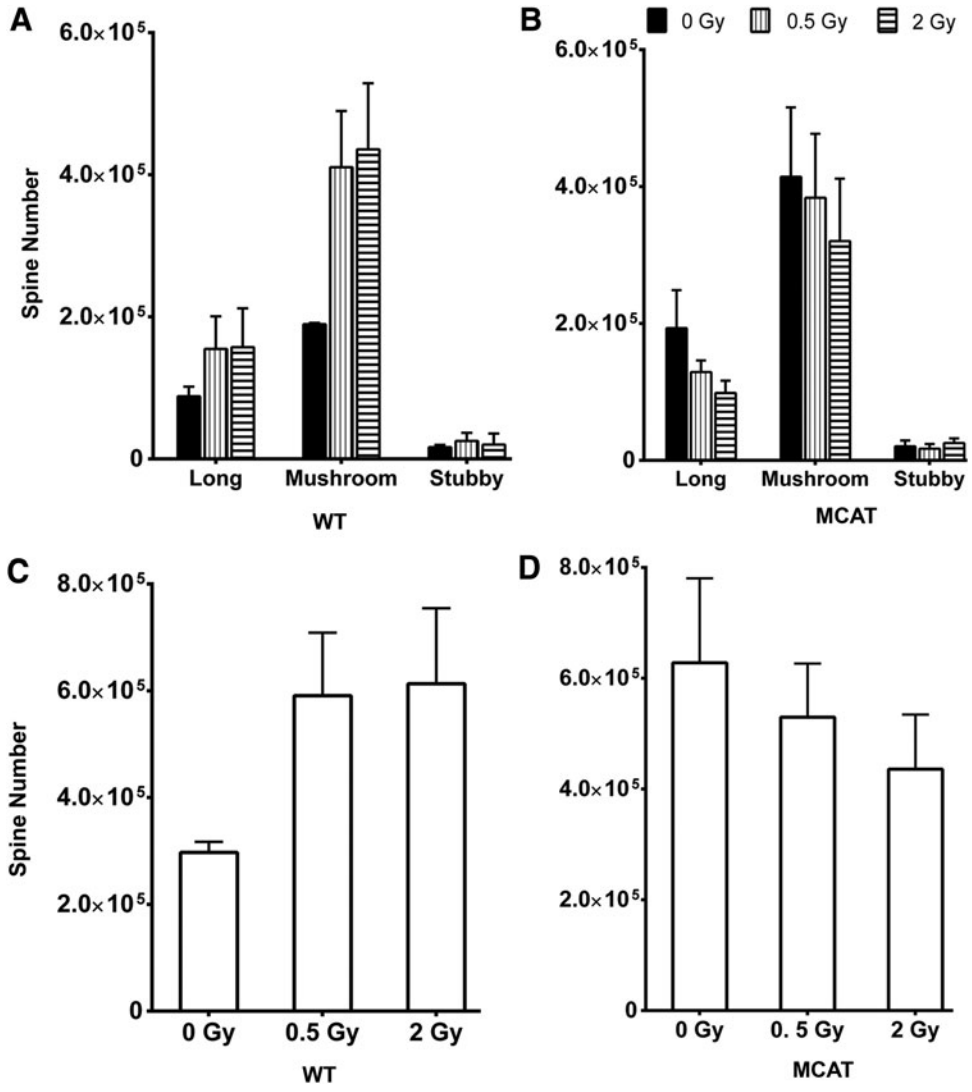

FIG. 6. Spine morphology and density in the CA1 of WT and MCAT mice. Spine morphology quantified at 6 weeks after proton exposure in WT **(A)** and MCAT **(B)** mice showed little effect of irradiation on long and stubby spine types. Trends (*albeit* not significant) were found for increased numbers of *mushroom* spine types in both genotypes after the 0.5 Gy dose. While differences between the genotypes were not found, overall spine densities trended higher in WT **(C)** and lower MCAT **(D)** mice after irradiation. All data are shown as the mean ± SEM derived from all animals ($n = 3$ animals, three sections per animal).

(40, 45) interventions designed to alter the oxidative environment point to the adverse effects of hydrogen peroxide on a variety of neural cell types in culture or within the intact CNS. Transgenic mouse models designed to manipulate levels of superoxide, a precursor of hydrogen peroxide derived from the activity of the three isoforms of SOD, have provided some intriguing insights into the interplay between certain reactive species in the brain. Targeted disruption of SOD1 (Cu/ZN SOD, intracellular), SOD2 (MnSOD, mitochondrial), or SOD3 (extracellular, EC-SOD) has been found to be neuroprotective after irradiation (21, 58), while overexpression of SOD2 or SOD3 was found to impair cognition (24, 63). Related studies have also found that overexpression of SOD1 or SOD3 can inhibit hippocampal LTP (22, 63).

The foregoing scenarios suggest that reduced hydrogen peroxide levels derived from SOD deficiency were beneficial to CNS functionality, while increased hydrogen peroxide levels derived from elevated SOD were deleterious to the CNS. High levels (0.5–5 m*M*) of hydrogen peroxide have been shown to inhibit synaptic plasticity in hippocampal slices, while low levels (1 μM) may be required for signaling in some forms of hippocampal plasticity (28, 29). Nonetheless, these previous findings corroborate many of the neuroprotective properties described here for MCAT mice, and suggest that antioxidant interventions targeted to reduce mitochondria hydrogen peroxide can have significant beneficial effects on the irradiated brain.

The functional significance of reducing mitochondrial hydrogen peroxide in the CNS after proton irradiation is clearly evident by the significant improvements in behavioral performance of MCAT compared with WT mice subjected to NOR and OiP tasks (Figs. 1 and 2). Proton irradiation induced significant deficits in these two cognitive tasks known to interrogate behavior dependent on both the medial prefrontal cortex (mPFC) and hippocampus. While these tasks are not entirely dependent on intact function of either of these subfields, evidence has indicated that these tasks are more sensitive to damage in the mPFC (2, 6). Relatively lower levels of damage (*via* lipopolysaccharide) to the circuitry of the mPFC elicit changes in NOR and OiP, while much higher levels of damage localized to the hippocampus are necessary to elicit performance decrement in these tasks (2, 6). Based on the irradiation paradigms used (whole body) and the low total doses delivered (≤ 2 Gy), the cognitive decrements reported here are more likely the result of damage to the mPFC, although contributions from damaged hippocampal circuitry

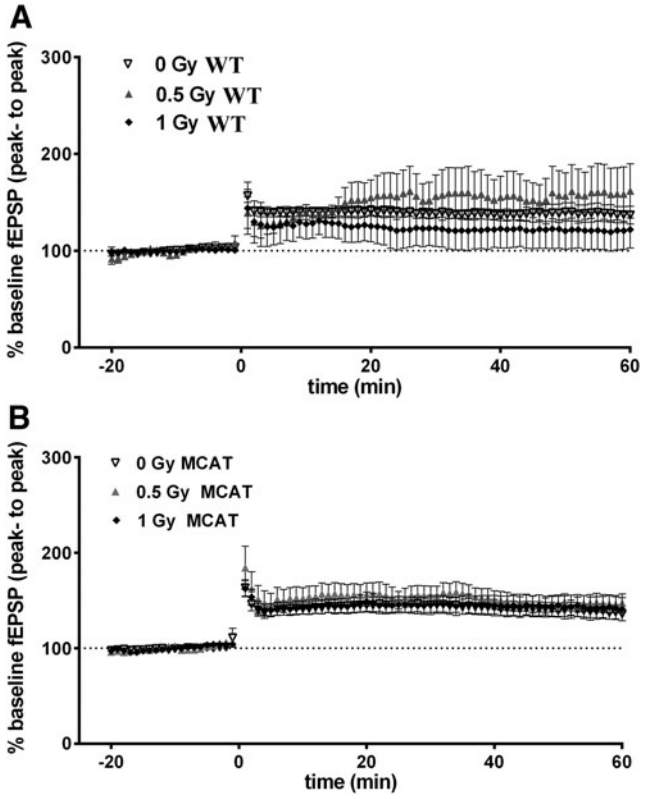

FIG. 7. LTP of the dendritic fEPSPs in hippocampal slices from WT and MCAT mice after proton irradiation. LTP was induced by HFS at time ''0'' and recorded in CA1 neurons for 60 min. fEPSPs were evaluated by peak-to-peak amplitude by Mobius™ built-in algorithm. **(A)** LTP measured in WT mice at 3 months after proton exposure shows a marked radiation-induced variability in LTP expression associated with fluctuations in the fEPSPs. **(B)** LTP time course measured in hippocampal slices of irradiated MCAT mice shows that LTP was relatively unaffected by irradiation, as peak-to-peak variations in the magnitude of the fEPSPs showed considerable stability in the MCAT background and resembled unirradiated (0 Gy) controls. All data are shown as the mean ± SEM derived from all animals (one to two slices per animal, $n = 16$/cohort). fEPSPs, field excitatory postsynaptic potentials; LTP, long-term potentiation. HFS, high-frequency stimulation.

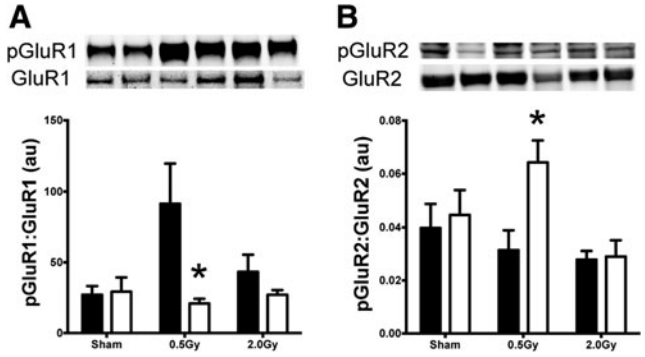

FIG. 8. Western blot analysis of hippocampal synaptic AMPAR phosphorylation at 6 weeks after proton irradiation. (A) 0.5 Gy proton exposure increased the ratio of pGLuR1 (S831) to total GLuR1 in WT mice ($*p < 0.05$), an effect that was abrogated in MCAT mice ($*p < 0.05$). **(B)** There was no treatment effect found for either dose of protons with regard to pGLuR2 (S845) to total GLuR2; however, a genotype effect was observed at 0.5 Gy ($*p < 0.05$). Data are presented as the average ratio of raw band intensity ± SEM. $n = 6$–8 per group. *Black bars* represent WT and white bars MCAT mice. AMPAR, AMPA receptor subunit.

cannot be conclusively ruled out. Cognitive data derived from irradiated WT mice clearly demonstrate the significant and adverse effects of proton exposure on the capability of animals to discriminate novelty through episodic or spatial learning and memory as assessed by NOR and OiP tasks, respectively. These decrements were not found in irradiated MCAT mice, where their behavioral assessments were indistinguishable from unirradiated controls. While it is possible that improved behavioral performance of MCAT animals might be due to certain developmental modifications of the brain in response to elevated MCAT activity, data most likely reflect the neuroprotective properties of reducing mitochondrial hydrogen peroxide after irradiation and prompt further investigations into the possible mechanisms underlying this effect.

Previous work from our group has identified the capability of ionizing radiation to compromise the structure of neurons in the hippocampus. Gamma ray and proton doses spanning 0.1–10.0 Gy have been found to cause significant, dose-responsive reductions in dendritic complexity and spine density lasting to at least 1 month postirradiation (11, 50, 51). These changes were coincident with reduced numbers of immature dendritic spines and alterations in synaptic protein levels (50, 51). Various forms of stress have been shown to compromise cognitive function and have clearly identified the importance of maintaining the integrity of the hippocampus at the structural and synaptic levels (27, 42). Based on the capability of proton irradiation to elicit performance decrements relying, in part, on hippocampal function, and based on a related finding which shows that MCAT mice exhibit improved neurogenesis, we chose to focus our morphometric analyses on hippocampal neurons.

To establish the impact of the MCAT transgene on neuronal morphology, brains from mice exposed to protons were Golgi stained and analyzed for structural changes in hippocampal neurons. In the DG, Sholl analysis of WT compared with MCAT mice revealed some significant reductions in dendritic intersections over shorter distances from the soma (30–60 μM) after 0.5 Gy, with more pronounced reductions over longer distances (130–170 μM) after 2.0 Gy (Supplementary Fig. S2). These data suggest that the MCAT transgene facilitates neuronal arborization, thereby protecting against radiation-induced reductions in dendritic complexity. While more robust structural changes to granule cell neurons expressing enhanced green fluorescent protein (EGFP) have been found after similar radiation paradigms, the method of Golgi only stains more mature neurons and may not provide the same level of sensitivity for quantifying ultrastructural changes in neurons after irradiation (50, 51).

Similar morphometric analyses carried out in the CA1 subfield revealed more extensive radiation-induced changes in pyramidal neurons. Sholl analysis of basal dendrites in WT and MCAT mice revealed no significant differences after 0 or 0.5 Gy (Supplementary Fig. S3), with some evidence of increased apical branching in unirradiated MCAT mice (Supplementary Fig. S4). However, in MCAT mice exposed to 2.0 Gy protons, basal dendritic extensions (70–100 μM)

from the soma were significantly longer, and measures of dendritic branch points, length, and overall dendritic complexity were significantly increased compared with WT mice (Figs. 3 and 4). WT mice exhibited significant reductions in both basal and apical dendritic complexity compared with MCAT mice (Fig. 3). The protective effects of the MCAT transgene were more pronounced in the apical dendritic tree, where dendritic intersections from the soma (30–110 μM) were significantly increased, and corresponded to significant increases in dendritic complexity and related structural endpoints (Figs. 3 and 4). A structural analysis of CA1 neurons in MCAT mice provides provocative evidence supporting the idea that the preservation of neuronal structure after irradiation is, in part, responsible for the neurocognitive benefits of reducing mitochondrial hydrogen peroxide.

Interestingly, the beneficial effects of MCAT expression did not extend to the level of dendritic spines, as changes in the type and density of spines on neurons within the DG and CA1 were not found to differ significantly after irradiation or between MCAT and WT mice (Figs. 5 and 6). Our previous work has found significant reductions in spine density and immature spine morphologies in the granule cell layer after exposure to gamma rays (50) or protons (51). While differences between the detection (EGFP expressing neurons *vs.* Golgi-Cox impregnated) and quantification (reconstruction *vs.* stereology) complicates a direct comparison of past and present data sets, current results suggest that the beneficial effects of MCAT expression are not due to a protection of dendritic spines.

LTP of excitatory postsynaptic potentials is a form of synaptic plasticity that can be induced by intense (tetanic) presynaptic stimulation. It has been a well-accepted cellular correlate of memory formation in the hippocampus. Previously, we showed that charged-particle radiation (*e.g.*, 600 MeV/n Fe) inhibits LTP in CA1 neurons at doses above 1 Gy without significantly affecting its time course (66). The effects of lower-dose charged particle exposure on LTP are more difficult to demonstrate, as fluctuations in LTP are commonly observed in slice preparations subjected to tetanic stimulation. Radiation-induced oxidative stress may also exacerbate LTP fluctuations by interfering with multiple signaling pathways that are known to be critical for hippocampal LTP. Irradiation may inhibit LTP by disrupting the function of NMDA receptors through elevated hydrogen peroxide, or promote LTP through superoxide generation (22, 30, 31, 63). Interestingly, hydrogen peroxide has been shown to have a dual role in LTP. While it inhibits hippocampal LTP in normal WT mice, it may enhance it in animals with altered metabolism of superoxide radical, an effect dependent on calcineurin activity and age (28, 29). Treatment of hippocampal slices with catalase can prevent hydrogen peroxide-induced decrements in slow onset, non-NMDA-dependent (muscarinic M2 receptor-mediated) LTP over a time course similar to that observed in our studies (3, 4). Thus, radiation-induced fluctuations in LTP reported here (Fig. 7A) are not entirely unexpected. Remarkably, the LTP amplitude in MCAT mice was unaffected by the radiation exposure, possibly due to improved decomposition of hydrogen peroxide and lower levels of radiation-induced oxidative stress over the protracted postirradiation interval (Fig. 7B). These data suggest that by reducing mitochondrial oxidative stress, electrophysiological responses may be stabilized after irradiation, thereby protecting CNS functionality.

AMPA receptor trafficking is critical for regulating various forms of synaptic plasticity in the CNS, and may be involved in the pathophysiology of radiation injury in the brain. In the adult hippocampus, AMPA receptors primarily consist of GluR1 and GluR2 (69). Phosphorylation of serines (S831 and S845) in the GluR1 subunit regulates ion channel properties and synaptic trafficking of AMPA receptors during hippocampal LTP (5, 7, 14, 17, 33, 41, 54). Dephosphorylation of GluR1 targets the subunit for endosome recycling during long-term depression (5). Elevated phospho-GluR1 in irradiated WT mice (Fig. 8A) may contribute to the variability in LTP, as ion channel properties change in response to multiple signaling cues that alter the tone of the irradiated hippocampus. The GluR1/2 heterodimer is known to regulate various forms of synaptic plasticity, and the presence of elevated phospho-GluR2 in MCAT mice (Fig. 8B) may render the hippocampus less susceptible to hyperexcitability due to reduced calcium permeability. The GluR2 subunit influences calcium permeability and excitotoxicity by affecting ion currents and synaptic reorganization (26). Reductions in overall GluR2 levels in the MCAT animals after irradiation may also promote neuroprotection by dampening excitotoxicity in response to low-dose (0.5 Gy) proton irradiation. Other reports corroborate these findings, where reductions in GluR2 have been found to elicit an adaptive mechanism to protect against ischemic damage (48, 62). Thus, the stabilizing effect of the MCAT transgene on LTP after irradiation may, in part, be explained by a change in the stoichiometric balance of GluR1/R2 subunits on AMPA receptors in the hippocampus.

This article documents the neuroprotective properties of overexpressing MCAT in a rodent model subjected to proton irradiation. Significant neurocognitive decrements in WT mice exposed to protons were not found in the MCAT transgenic background. Improved cognition after irradiation was associated with longer granule cell dendrites in the DG, and a preservation of basal and apical dendritic complexity in the CA1 subfield of the hippocampus. Radiation-induced changes in LTP were stabilized in MCAT mice that coincided with changes in the proportion of phosphorylated GluR1/R2 AMPA receptor subunits. These data point to several potentially promising interventions for minimizing the adverse effects of irradiation on the brain. Drugs targeted to minimize mitochondrial-derived ROS protect host dendritic structure or enhance the ratio of phospho-GluR2:GluR1 may provide some control over the progression and/or severity of radiation-induced cognitive dysfunction. As the number of patients suffering from neurocognitive sequelae associated with cranial radiotherapy continues to grow, and evidence mounts regarding related adverse cognitive complications derived from lower occupational exposures, the need to move novel strategies into practice becomes increasingly urgent. The findings presented here may prove useful in this regard, as our data point to the importance of redox balance in the CNS, and how an intervention designed to minimize oxidative stress can impart such marked neuroprotective effects to the irradiated brain.

Materials and Methods

Animals and irradiation

All animal procedures were carried out in accordance with NIH and IACUC guidelines. Transgenic mice overexpressing human catalase targeted to the mitochondria [MCAT,

founder strain B6.C3H-Tg(MCAT)4033Wcl] backcrossed onto the C57BL/6J (WT) background were a kind gift from Drs. Warren Ladiges and Peter Rabinovitch (University of Washington, Seattle, WA). Male mice (2 months old) were exposed to whole body irradiation using 150 MeV plateau phase protons at a dose rate of 0.5 Gy/min generated at the synchrotron accelerator at the Loma Linda University (CA, USA) Proton Treatment Facility. A total of 96 mice were used in this study and groups were divided as 0, 0.503 ± 0.006, and 2.006 ± 0.005 Gy (WT and MCAT, $n = 16$ each) at a dose rate of 0.45–0.48 Gy/min. Cognitive testing was initiated at 1 month after irradiation, and once concluded, animals were sacrificed for the preparation of tissues for immunohistochemical, biochemical, and morphometric analyses. For the assessment of catalase activity, brains were prepared as previously described (70). Separate cohorts of animals (WT and MCAT, $n = 16$) were irradiated (0, 0.500 ± 0.000 and 1.007 ± 0.011 Gy) with protons independently for electrophysiological determinations after 90 days.

Behavioral testing

To determine whether overexpression of MCAT can recover from cognitive deficits caused by low doses of proton radiation, control and MCAT mice ($n = 16$ per group, 96 total) were given 0, 0.5, or 2.0 Gy and evaluated 4 weeks later on the NOR and OiP testing arenas. NOR and OiP rely on intact hippocampal function, while NOR is a measure of episodic memory, OiP is a test of spatial memory (2, 6). Due to the large numbers of mice, all treatment groups were randomly divided into three cohorts and behavior was conducted over the course of 3 weeks.

Behavior was conducted in a dimly lit, dedicated room separated from housing. Four arena boxes made of acrylic ($30 \times 30 \times 30$ cm) were placed two by two, layered with fresh, autoclaved, corncob bedding, and placed on the floor. Care was taken to keep the arenas in exactly the same location, and mice were never rotated to other arenas during the duration of the behavior testing. A camera was mounted above the arenas to record each trial. Each arena was thoroughly cleaned between trials with 70% ethanol, and fresh bedding was used to eliminate distinguishing olfactory cues.

NOR test

The NOR test was administered after 3 days of habituation (10 min/day). Objects to be distinguished were made of a similar plastic material but varied in color, shape, and size. To ensure that objects were in exactly the same position for each trial, magnets were used to hold them in place ~ 7 cm from opposing corners and 16 cm apart. During the testing day, mice were exposed to two duplicate objects within the arena for 5 min (familiarization). They were then allowed to rest for 5 min in their home cage within the behavioral room while the objects were cleaned (70% ethanol), and a novel object was added. Mice were then returned to the arena for 5 min, where they explored the familiar and novel object (testing). These objects were not used in subsequent testing.

Trials were later hand scored by an individual blinded to the experimental groups and calculated by using the discrimination index:

$$\frac{\text{Time spent exploring novel object}}{\text{total exploration time}} - \frac{\text{Time spent exploring familiar object}}{\text{total exploration time}} \times 100$$

A positive score is counted when the nose of the mouse is within 1 cm and pointed in the direction of the object. Time was not scored for mice that were near but not facing the object.

OiP test

The week after cessation of NOR testing, mice were habituated again to their arenas (10 min/day) for 2 consecutive days. On the third day, mice were exposed to four objects of varying size, color, and shape for 5 min (familiarization). Mice were then allowed to rest for 5 min in their home cage within the same room as the arenas. Objects were cleaned with 70% ethanol, and two of the four objects switched locations. The objects were counter balanced between the groups to assure there were no inherent preferences to a particular object. Mice were returned to the arenas for 5 min of exploration (testing). Trials were later hand scored by an individual blinded to the experimental groups and calculated by using the discrimination index as described earlier. Positive scores were calculated based on the same criteria detailed for the NOR task earlier.

Golgi staining and tissue preparation

Animals subjected to behavioral testing were segregated differentially for the preparation of neural tissues destined for specific analyses. For biochemical analyses and Golgi staining, 10 mice per group were anesthetized in a chamber saturated with isoflurane vapors and perfused with 25 ml of cold normal saline.

The brains were carefully extracted and cut in half along the midsagittal planes. The right hemisphere of the brain was immediately subjected to the Bioenno Tech superGolgi kit for Golgi-Cox method of staining. The samples were impregnated with the potassium dichromate and mercuric chloride solution at room temperature for 11 days. After immersion in the postimpregnation buffer for 2 days, brains were serially sectioned at 100 μm using a vibrating microtome and sections were collected in chilled mounting buffer. The sections were mounted on 0.3% gelatin-coated slides, washed in 0.01 *M* phosphate-buffered saline (PBS) buffer (pH 7.4) with Triton X-100 (0.3%), and stained with ammonium hydroxide solution (provided in the kit). After staining and washing, slides were gradually dehydrated through a series of increasing alcohol concentrations, then with xylene and finally mounted in Permount™ (Fisher) for analysis.

Morphometry

Morphometric analysis of apical and basal dendrites was conducted on neurons within the DG (both blades) and CA1 (including subiculum) subfields of Golgi impregnated brain sections containing the hippocampus. All analyses were conducted blinded from coded slides. Neurons were identified within specific subfields of the hippocampus for tracing at a low magnification ($20\times$). Five representative neurons were traced per region, from each animal. The candidate neurons that satisfied the following criteria were chosen for analysis in each of the experimental groups: (i) presence of

untruncated dendrites; (ii) consistent and dark Golgi staining along the entire extent of the dendrites; (iii) minimal structural overlap with neighboring neurons; and (iv) majority of terminal dendritic fields ended within the section (*i.e.*, not severed during sectioning) (23, 55). Neurons satisfying the foregoing criteria were traced under 60×, using a computerized stage, and Neurolucida software (Ver. 11; Microbrightfield, Inc.).

Morphological parameters that were quantified included total dendritic length, dendritic complexity index (DCI), number of branch points, and Sholl analysis, performed using the Neuroexplorer component of the Neurolucida program. DCI was determined by the following equation: DCI = (Σ branch tip orders + # branch tips) × (total dendritic length/total number of primary dendrites). A bifurcation of a dendritic branch represents a branch point (*e.g.*, when a branch divides into two suborders). The Sholl analysis provides a synthetic representation of the distance of dendrites from the soma. The distance between each radius was set to 10 μm, and the starting point was located at the cell body. The number of dendrite intersections with Sholl circles was counted. In the CA1 area, apical and basal dendrites were analyzed separately.

Dendritic spines

Dendritic spines were quantified using unbiased stereology from the same set of Golgi impregnated tissues used for morphometric analyses. Serial sections (every third) taken through the entire hippocampus were selected to analyze potential differences in the susceptibility of morphologically distinct spines to proton irradiation and MCAT expression. Distinct subclasses of spines were categorized and quantified separately. For different cell layers of the hippocampus (stratum radiatum, lacunosum-molecular layer) spines were counted separately. Spines were counted from 15 to 20 random but representative frames (each measuring $10 \times 10\ \mu m^2$) placed over each of the cell layers. All spines were counted using the 100× oil immersion lens with 1.5× camera zoom. The numbers of frames for each section were determined by using the optical fractionator (StereoInvestigator; MBF). Spine quantification from optical fractionator sampling was optimized to yield about 10–25 counted spines per frame yielding Gundersen error coefficients < 0.10.

Hippocampal slice preparation and in vitro *electrophysiological recordings*

Animals were deeply anesthetized with 3.5% isoflurane and sacrificed for *in vitro* electrophysiology at 90 ± 10 days after irradiation. Transverse hippocampal slices were prepared using a McIlwain tissue chopper from the rostro-medial part of the hippocampus and incubated at 33.0°C ± 0.5°C in artificial cerebrospinal fluid in accordance with standard protocols (66). The MED64 multielectrode array (Panasonic) was used in conjunction with a 16×4 channel divider (MED-B02; AlfaMED) and multi-electrode MED64 chips (type P210A; AlfaMED) to evoke and record fEPSPs in CA1 neurons as previously described (53). The fEPSP peak-to-peak amplitudes were measured by Mobius™ Ver. Win7.0.3.9 (WitWerx, Inc., AlphaMed) using built-in algorithms. Measures were exported to Excel (Microsoft) for further data processing. Synaptic plasticity was evaluated by induction of LTP of the fEPSP. Stimulation intensity (SI) evoking 30% of the maximal fEPSP ($SI_{30\%}$) was used to record baseline responses for 20 min. LTP were then induced by HFS (2 trains of 100 pulses at 100 Hz separated by 20 s). One minute later, normal stimulation was resumed (at $SI_{30\%}$) and recordings were continued for the next 60 min. LTP of the fEPSP was expressed as a percentage change relative to the fEPSP in the baseline period. All data are shown as the mean ± SEM derived from all animals (one to two slices per animal). All the statistical analyses were performed using repeated-measures two-way ANOVA in GraphPad Prism software.

Biochemical analyses of synaptosomes

Synaptosome-enriched fractions were prepared from isolated hippocampi as previously described (19, 61). Briefly, tissues were homogenized in 200 μl of buffer (10 m*M* Tris, 300 m*M* sucrose, with protease inhibitors) on ice using a Dounce homogenizer. The resulting homogenate was processed further using a syringe equipped with a 21.5-gauge needle. Homogenates were immediately transferred to 1.5 ml conical tubes and centrifuged at 5000 *g* for 5 min at 4°C, yielding the first pellet (P1) and supernatant (S1) fractions. The S1 fraction was re-centrifuged at 13,000 *g* for 30 min at 4°C, yielding the second pellet (P2) and supernatant (S2) fractions. The S2 fraction was aspirated from the P2 fraction, which was immediately resuspended in PBS containing protease inhibitors. After determination of total protein concentration (standard BCA assay; Pierce), samples containing 10 μg of total protein were loaded onto 4%–15% sodium dodecyl sulfate gels (Bio-Rad) for electrophoresis and subsequent transfer onto nitrocellulose membranes. Immunoblots were probed for GluR1 (1:750; Millipore), p-GluR1 (s831; 1:1000; Millipore), GluR2 (1:500; Millipore), p-GluR2 (s845, 1:500; Millipore), and GAPDH (Sigma). Incubation and analysis of blots were performed as previously detailed (46) using the LiCor Odyssey near-infrared system.

Statistics

All data are shown as mean ± SEM. Statistical analyses were performed using repeated-measures two-way ANOVA in GraphPad Prism software (v.6.0). Significance was assessed at $p < 0.05$ and followed with multiple *post hoc* comparisons of cognitive (Dunnett's test) and electrophysiological (Tukey's) data. For measures of dendritic intersections, a mixed factors ANOVA tested for the effects of genotype (between subjects variable) and distance from the cell body (Sholl radius, repeated measures variable) followed by Fisher LSD *post hoc* tests. For comparisons between wild-type and MCAT mice, dendritic length, branch points, and DCI parametric two-tailed unpaired *t*-test were performed with Welch's correction.

Acknowledgments

This work was supported by National Institutes of Health NINDS Grant R01 NS074388 (C.L.L.) and by NASA Grants NNX13AD59G (C.L.L.) and NNX10AD59G (S.R., R.V., G.A.N., A.A., C.L.L.). The authors thank Mary Campbell-Beachler for excellent technical assistance with electrophysiological recordings and data analyses.

Author Disclosure Statement

No competing financial interests exist.

References

1. Acharya MM, Lan ML, Kan VH, Patel NH, Giedzinski E, Tseng BP, and Limoli CL. Consequences of ionizing radiation-induced damage in human neural stem cells. *Free Radic Biol Med* 49: 1846–1855, 2010.
2. Aggleton JP and Brown MW. Contrasting hippocampal and perirhinal cortex function using immediate early gene imaging. *Q J Exp Psychol B* 58: 218–233, 2005.
3. Auerbach JM and Segal M. A novel cholinergic induction of long-term potentiation in rat hippocampus. *J Neurophysiol* 72: 2034–2040, 1994.
4. Auerbach JM and Segal M. Peroxide modulation of slow onset potentiation in rat hippocampus. *J Neurosci* 17: 8695–8701, 1997.
5. Banke TG, Bowie D, Lee H, Huganir RL, Schousboe A, and Traynelis SF. Control of GluR1 AMPA receptor function by cAMP-dependent protein kinase. *J Neurosci* 20: 89–102, 2000.
6. Barker GR and Warburton EC. When is the hippocampus involved in recognition memory? *J Neurosci* 31: 10721–10731, 2011.
7. Barria A, Muller D, Derkach V, Griffith LC, and Soderling TR. Regulatory phosphorylation of AMPA-type glutamate receptors by CaM-KII during long-term potentiation. *Science* 276: 2042–2045, 1997.
8. Brenner DJ, Doll R, Goodhead DT, Hall EJ, Land CE, Little JB, Lubin JH, Preston DL, Preston RJ, Puskin JS, Ron E, Sachs RK, Samet JM, Setlow RB, and Zaider M. Cancer risks attributable to low doses of ionizing radiation: assessing what we really know. *Proc Natl Acad Sci U S A* 100: 13761–13766, 2003.
9. Britten RA, Davis LK, Johnson AM, Keeney S, Siegel A, Sanford LD, Singletary SJ, and Lonart G. Low (20 cGy) doses of 1 GeV/u (56)Fe—particle radiation lead to a persistent reduction in the spatial learning ability of rats. *Radiat Res* 177: 146–151, 2012.
10. Butler JM, Rapp SR, and Shaw EG. Managing the cognitive effects of brain tumor radiation therapy. *Curr Treat Options Oncol* 7: 517–523, 2006.
11. Chakraborti A, Allen A, Allen B, Rosi S, and Fike JR. Cranial irradiation alters dendritic spine density and morphology in the hippocampus. *PLoS One* 7: e40844, 2012.
12. Cucinotta FA and Durante M. Cancer risk from exposure to galactic cosmic rays: implications for space exploration by human beings. *Lancet Oncol* 7: 431–435, 2006.
13. Dai DF, Santana LF, Vermulst M, Tomazela DM, Emond MJ, MacCoss MJ, Gollahon K, Martin GM, Loeb LA, Ladiges WC, and Rabinovitch PS. Overexpression of catalase targeted to mitochondria attenuates murine cardiac aging. *Circulation* 119: 2789–2797, 2009.
14. Derkach V, Barria A, and Soderling TR. Ca2+/calmodulin-kinase II enhances channel conductance of alpha-amino-3-hydroxy-5-methyl-4-isoxazolepropionate type glutamate receptors. *Proc Natl Acad Sci U S A* 96: 3269–3274, 1999.
15. Douw L, Klein M, Fagel SS, van den Heuvel J, Taphoorn MJ, Aaronson NK, Postma TJ, Vandertop WP, Mooij JJ, Boerman RH, Beute GN, Sluimer JD, Slotman BJ, Reijneveld JC, and Heimans JJ. Cognitive and radiological effects of radiotherapy in patients with low-grade glioma: long-term follow-up. *Lancet Neurol* 8: 810–818, 2009.
16. Durante M and Cucinotta FA. Heavy ion carcinogenesis and human space exploration. *Nat Rev Cancer* 8: 465–472, 2008.
17. Esteban JA. AMPA receptor trafficking: a road map for synaptic plasticity. *Mol Interv* 3: 375–385, 2003.
18. Feeney CJ, Frantseva MV, Carlen PL, Pennefather PS, Shulyakova N, Shniffer C, and Mills LR. Vulnerability of glial cells to hydrogen peroxide in cultured hippocampal slices. *Brain Res* 1198: 1–15, 2008.
19. Ferguson AR, Christensen RN, Gensel JC, Miller BA, Sun F, Beattie EC, Bresnahan JC, and Beattie MS. Cell death after spinal cord injury is exacerbated by rapid TNF alpha-induced trafficking of GluR2-lacking AMPARs to the plasma membrane. *J Neurosci* 28: 11391–11400, 2008.
20. Fike JR, Rosi S, and Limoli CL. Neural precursor cells and central nervous system radiation sensitivity. *Semin Radiat Oncol* 19: 122–132, 2009.
21. Fishman K, Baure J, Zou Y, Huang TT, Andres-Mach M, Rola R, Suarez T, Acharya M, Limoli CL, Lamborn KR, and Fike JR. Radiation-induced reductions in neurogenesis are ameliorated in mice deficient in CuZnSOD or MnSOD. *Free Radic Biol Med* 47: 1459–1467, 2009.
22. Gahtan E, Auerbach JM, Groner Y, and Segal M. Reversible impairment of long-term potentiation in transgenic Cu/Zn-SOD mice. *Eur J Neurosci* 10: 538–544, 1998.
23. Harris KM, Jensen FE, and Tsao B. Three-dimensional structure of dendritic spines and synapses in rat hippocampus (CA1) at postnatal day 15 and adult ages: implications for the maturation of synaptic physiology and long-term potentiation. *J Neurosci* 12: 2685–2705, 1992.
24. Hu D, Cao P, Thiels E, Chu CT, Wu GY, Oury TD, and Klann E. Hippocampal long-term potentiation, memory, and longevity in mice that overexpress mitochondrial superoxide dismutase. *Neurobiol Learn Mem* 87: 372–384, 2007.
25. Huang TT, Zou Y, and Corniola R. Oxidative stress and adult neurogenesis—effects of radiation and superoxide dismutase deficiency. *Semin Cell Dev Biol* 23: 738–744, 2012.
26. Iihara K, Joo DT, Henderson J, Sattler R, Taverna FA, Lourensen S, Orser BA, Roder JC, and Tymianski M. The influence of glutamate receptor 2 expression on excitotoxicity in Glur2 null mutant mice. *J Neurosci* 21: 2224–2239, 2001.
27. Ivy AS, Rex CS, Chen Y, Dube C, Maras PM, Grigoriadis DE, Gall CM, Lynch G, and Baram TZ. Hippocampal dysfunction and cognitive impairments provoked by chronic early-life stress involve excessive activation of CRH receptors. *J Neurosci* 30: 13005–13015, 2010.
28. Kamsler A and Segal M. Hydrogen peroxide modulation of synaptic plasticity. *J Neurosci* 23: 269–276, 2003.
29. Kamsler A and Segal M. Paradoxical actions of hydrogen peroxide on long-term potentiation in transgenic superoxide dismutase-1 mice. *J Neurosci* 23: 10359–10367, 2003.
30. Klann E. Cell-permeable scavengers of superoxide prevent long-term potentiation in hippocampal area CA1. *J Neurophysiol* 80: 452–457, 1998.
31. Klann E, Roberson ED, Knapp LT, and Sweatt JD. A role for superoxide in protein kinase C activation and induction of long-term potentiation. *J Biol Chem* 273: 4516–4522, 1998.
32. Leach JK, Black SM, Schmidt-Ullrich RK, and Mikkelsen RB. Activation of constitutive nitric-oxide synthase activity is an early signaling event induced by ionizing radiation. *J Biol Chem* 277: 15400–15406, 2002.
33. Lee HK, Barbarosie M, Kameyama K, Bear MF, and Huganir RL. Regulation of distinct AMPA receptor phosphorylation

sites during bidirectional synaptic plasticity. *Nature* 405: 955–959, 2000.
34. Lewen A, Matz P, and Chan PH. Free radical pathways in CNS injury. *J Neurotrauma* 17: 871–890, 2000.
35. Liao AC, Craver BM, Tseng BP, Tran KK, Parihar VK, Acharya MM, and Limoli CL. Mitochondrial-targeted human catalase affords neuroprotection from proton irradiation. *Radiat Res* 180: 1–6, 2013.
36. Limoli C, Giedzinski E, Rola R, Otsuka S, Palmer T, and Fike J. Radiation response of neural precursor cells: linking cellular sensitivity to cell cycle checkpoints, apoptosis and oxidative stress. *Radiat Res* 161: 17–27, 2004.
37. Limoli CL, Giedzinski E, Baure J, Rola R, and Fike JR. Redox changes induced in hippocampal precursor cells by heavy ion irradiation. *Radiat Environ Biophys* 46: 167–172, 2007.
38. Limoli CL, Rola R, Giedzinski E, Mantha S, Huang TT, and Fike JR. Cell-density-dependent regulation of neural precursor cell function. *Proc Natl Acad Sci U S A* 101: 16052–16057, 2004.
39. Lonart G, Parris B, Johnson AM, Miles S, Sanford LD, Singletary SJ, and Britten RA. Executive function in rats is impaired by low (20 cGy) doses of 1 GeV/u (56)Fe particles. *Radiat Res* 178: 289–294, 2012.
40. Mailly F, Marin P, Israel M, Glowinski J, and Premont J. Increase in external glutamate and NMDA receptor activation contribute to H2O2-induced neuronal apoptosis. *J Neurochem* 73: 1181–1188, 1999.
41. Mammen AL, Kameyama K, Roche KW, and Huganir RL. Phosphorylation of the alpha-amino-3-hydroxy-5-methylisoxazole4-propionic acid receptor GluR1 subunit by calcium/calmodulin-dependent kinase II. *J Biol Chem* 272: 32528–32533, 1997.
42. Maras PM, Molet J, Chen Y, Rice C, Ji SG, Solodkin A, and Baram TZ. Preferential loss of dorsal-hippocampus synapses underlies memory impairments provoked by short, multimodal stress. *Mol Psychiatry* 19: 811–822, 2014.
43. Meyers CA. Neurocognitive dysfunction in cancer patients. *Oncology (Williston Park)* 14: 75–79, 2000; discussion 79, 81–72, 85.
44. Meyers CA and Brown PD. Role and relevance of neurocognitive assessment in clinical trials of patients with CNS tumors. *J Clin Oncol* 24: 1305–1309, 2006.
45. Milton NG. Inhibition of catalase activity with 3-aminotriazole enhances the cytotoxicity of the Alzheimer's amyloid-beta peptide. *Neurotoxicology* 22: 767–774, 2001.
46. Morganti JM, Nash KR, Grimmig BA, Ranjit S, Small B, Bickford PC, and Gemma C. The soluble isoform of CX3CL1 is necessary for neuroprotection in a mouse model of Parkinson's disease. *J Neurosci* 32: 14592–14601, 2012.
47. Niizuma K, Endo H, and Chan PH. Oxidative stress and mitochondrial dysfunction as determinants of ischemic neuronal death and survival. *J Neurochem* 109 Suppl 1: 133–138, 2009.
48. Oguro K, Oguro N, Kojima T, Grooms SY, Calderone A, Zheng X, Bennett MV, and Zukin RS. Knockdown of AMPA receptor GluR2 expression causes delayed neurodegeneration and increases damage by sublethal ischemia in hippocampal CA1 and CA3 neurons. *J Neurosci* 19: 9218–9227, 1999.
49. Olsen RH, Johnson LA, Zuloaga DG, Limoli CL, and Raber J. Enhanced hippocampus-dependent memory and reduced anxiety in mice over-expressing human catalase in mitochondria. *J Neurochem* 2013. DOI: 10.1111/jnc.12187.
50. Parihar VK and Limoli CL. Cranial irradiation compromises neuronal architecture in the hippocampus. *Proc Natl Acad Sci U S A* 110: 12822–12827, 2013.
51. Parihar VK, Pasha J, Tran KK, Craver BM, Acharya MM, and Limoli CL. Persistent changes in neuronal structure and synaptic plasticity caused by proton irradiation. *Brain Struct Func* 2014 [Epub ahead of print]; DOI: 10.1007/s00429-014-0709-9.
52. Preston RJ, Boice JD, Jr., Brill AB, Chakraborty R, Conolly R, Hoffman FO, Hornung RW, Kocher DC, Land CE, Shore RE, and Woloschak GE. Uncertainties in estimating health risks associated with exposure to ionising radiation. *J Radiol Prot* 33: 573–588, 2013.
53. Raber J, Rudobeck E, Campbell-Beachler M, Allen A, Rosi S, Nelson G, Ramachandran S, Turner J, Fike J, and Vlkolinsky R. ^{28}Silicon radiation-induced enhancement of synaptic plasticity in the hippocampus of naive and cognitively tested mice. *Radiat Res* 181: 362–368, 2014.
54. Roche KW, O'Brien RJ, Mammen AL, Bernhardt J, and Huganir RL. Characterization of multiple phosphorylation sites on the AMPA receptor GluR1 subunit. *Neuron* 16: 1179–1188, 1996.
55. Rodriguez A, Ehlenberger DB, Dickstein DL, Hof PR, and Wearne SL. Automated three-dimensional detection and shape classification of dendritic spines from fluorescence microscopy images. *PLoS One* 3: e1997, 2008.
56. Rola R, Otsuka S, Obenaus A, Nelson GA, Limoli CL, VandenBerg SR, and Fike JR. Indicators of hippocampal neurogenesis are altered by 56Fe-particle irradiation in a dose-dependent manner. *Radiat Res* 162: 442–446, 2004.
57. Rola R, Raber J, Rizk A, Otsuka S, VandenBerg SR, Morhardt DR, and Fike JR. Radiation-induced impairment of hippocampal neurogenesis is associated with cognitive deficits in young mice. *Exp Neurol* 188: 316–330, 2004.
58. Rola R, Zou Y, Huang TT, Fishman K, Baure J, Rosi S, Milliken H, Limoli CL, and Fike JR. Lack of extracellular superoxide dismutase (EC-SOD) in the microenvironment impacts radiation-induced changes in neurogenesis. *Free Radic Biol Med* 42: 1133–1145, 2007; discussion 1131–1132.
59. Schriner SE, Linford NJ, Martin GM, Treuting P, Ogburn CE, Emond M, Coskun PE, Ladiges W, Wolf N, Van Remmen H, Wallace DC, and Rabinovitch PS. Extension of murine life span by overexpression of catalase targeted to mitochondria. *Science* 308: 1909–1911, 2005.
60. Sholl DA. Dendritic organization in the neurons of the visual and motor cortices of the cat. *J Anat* 87: 387–406, 1953.
61. Stuck ED, Christensen RN, Huie JR, Tovar CA, Miller BA, Nout YS, Bresnahan JC, Beattie MS, and Ferguson AR. Tumor necrosis factor alpha mediates GABA(A) receptor trafficking to the plasma membrane of spinal cord neurons *in vivo*. *Neural Plast* 2012: 261345, 2012.
62. Tanaka H, Calderone A, Jover T, Grooms SY, Yokota H, Zukin RS, and Bennett MV. Ischemic preconditioning acts upstream of GluR2 down-regulation to afford neuroprotection in the hippocampal CA1. *Proc Natl Acad Sci U S A* 99: 2362–2367, 2002.
63. Thiels E, Urban NN, Gonzalez-Burgos GR, Kanterewicz BI, Barrionuevo G, Chu CT, Oury TD, and Klann E.

Impairment of long-term potentiation and associative memory in mice that overexpress extracellular superoxide dismutase. *J Neurosci* 20: 7631–7639, 2000.
64. Tofilon PJ and Fike JR. The radioresponse of the central nervous system: a dynamic process. *Radiat Res* 153: 354–370, 2000.
65. Tseng BP, Giedzinski E, Izadi A, Suarez T, Lan ML, Tran KK, Acharya MM, Nelson GA, Raber J, Parihar VK, and Limoli CL. Functional consequences of radiation-induced oxidative stress in cultured neural stem cells and the brain exposed to charged particle irradiation. *Antioxid Redox Signal* 20: 1410–1422, 2013.
66. Vlkolinsky R, Krucker T, Smith AL, Lamp TC, Nelson GA, and Obenaus A. Effects of lipopolysaccharide on 56Fe-particle radiation-induced impairment of synaptic plasticity in the mouse hippocampus. *Radiat Res* 168: 462–470, 2007.
67. Ward JF, Jones GDD, and Milligan JR. Biological consequences of non-homogeneous energy deposition by ionising radiation. *Radiat Prot Dosim* 52: 271–276, 1994.
68. Ward JF, Webb CF, Limoli CL, and Milligan JR. DNA lesions produced by ionizing radiation: locally multiply damaged sites. In: *Ionizing Radiation Damage to DNA: Molecular Aspects*, edited by Wallace SS and Painter RB. New York: Wiley-Liss, 1990, pp. 43–50.
69. Wenthold RJ, Petralia RS, Blahos J, II, and Niedzielski AS. Evidence for multiple AMPA receptor complexes in hippocampal CA1/CA2 neurons. *J Neurosci* 16: 1982–1989, 1996.
70. Xie W, Wu Q, Kania-Korwel I, Tharappel JC, Telu S, Coleman MC, Glauert HP, Kannan K, Mariappan SV, Spitz DR, Weydert J, and Lehmler HJ. Subacute exposure to N-ethyl perfluorooctanesulfonamidoethanol results in the formation of perfluorooctanesulfonate and alters superoxide dismutase activity in female rats. *Arch Toxicol* 83: 909–924, 2009.

Address correspondence to:
Prof. Charles L. Limoli
Department of Radiation Oncology
University of California, Irvine
Medical Sciences I
Room B-146B
Irvine, CA 92697-2695

E-mail: climoli@uci.edu

Date of first submission to ARS Central, March 26, 2014; date of final revised submission, June 11, 2014; date of acceptance, June 20, 2014.

Abbreviations Used

AMPAR = AMPA receptor subunits
ANOVA = analysis of variance
CNS = central nervous system
DCI = dendritic complexity index
DG = dentate gyrus
EGFP = enhanced green fluorescent protein
fEPSP = field excitatory postsynaptic potentials
Gy = gray
HFS = high-frequency stimulation
LSD = least significant difference
LTP = long-term potentiation
MCAT = mitochondrial catalase
mPFC = medial prefrontal cortex
NOR = novel object recognition
OiP = object in place
PBS = phosphate-buffered saline
ROS = reactive oxygen species
SI = stimulation intensity
SOD = superoxide dismutase
WT = wild type